FILTER BANKS FOR HEARING AIDS APPLYING SUBBAND AMPLIFICATION: A COMPARISON OF DIFFERENT SPECIFICATION AND DESIGN APPROACHES

Daniel Alfsmann, Heinz G. Göckler and Thomas Kurbiel

Digital Signal Processing Group (DISPO), Ruhr-Universität Bochum, 44780 Bochum, Germany
phone: + (49) 234 32-27585, fax: -07585, email: {alfsmann, goeckler, kurbiel}@nt.rub.de, web: www.dsv.rub.de

ABSTRACT

Hearing instruments employ filter bank systems (FBS) to subdivide the microphone signal into subband signals. To reduce overall computation, decimation is applied, which inevitably induces disturbance. First, these effects are analysed in detail. Then, we postulate application specific FBS requirements in view of extensive subband signal amplification. Next, we compare four different prototype filter specification and design approaches for oversampling complex-modulated FBS with respect to the postulated requirements. Finally, we present design examples applying these approaches. Thus, we explicitly demonstrate the impact of subband signal amplification on the FBS characteristics.

1. INTRODUCTION

A hearing instrument (HI) is a device to enhance the intelligibility of speech in everyday environments, especially for the hearing impaired user. Usually, hearing loss is not flat versus frequency. As a result, a hearing aid must individually compensate for each personal hearing loss in a frequency-selective manner. To this end, the audible spectrum to be processed must be decomposed into subband signals of suitable bandwidths that are amenable to subband signal processing (SSP) separately.

In modern hearing instruments, digital filter bank systems (FBS) are commonly used for frequency-selective signal decomposition. This approach requires a digital analysis filter bank (AFB) with sufficient frequency resolution cascaded with a subsequent synthesis filter bank (SFB) for reconstruction of the individually manipulated subband signals. Since SSP (e.g. amplification, noise reduction, compression) becomes more and more challenging [1, 2, 3], highly efficient and energy-saving processing is only feasible with *decimated* subband signals. A typical example of most efficient decimating FBS are complex-modulated (DFT) filter banks with polyphase implementation of the FIR prototype filters [4, 5].

Any decimating FBS always contributes multirate disturbance (aliasing and imaging) to the subband and output signals, respectively. In contrast to most common approaches [4, 5] that apply aliasing compensation and (near) perfect reconstruction (PR), FBS for hearing instruments cannot exploit these techniques as a consequence of extensive SSP, especially due to highly differing subband signal amplifications of up to 60 dB [3, 6, 7]. Hence, complex-modulated FBS for HI must be designed for *oversampled* subband signals, and with sufficiently high AFB and SFB stopband attenuation to control aliasing and imaging disturbance. The integer subband signal oversampling factor is defined by $\mathscr{O} = I/M > 1$, where I and $M \in \mathbb{N}$ represent the number of filter bank channels and the decimation factor, respectively.

The objective of this contribution is to investigate the particular conditions and requirements of oversampling FBS for HI and, thus, to derive suitable specifications ensuring that the FBS designed accordingly can essentially meet all needs. In this study, we clearly distinguish between the two sources of multirate disturbance, aliasing and imaging. In prescribing a desired signal quality (signal-to-distortion ratio) predominantly at the FBS output port, it turns out that the AFB and SFB prototype filters have to be specified in a different way, which generally results in different FIR filter lengths. In addition, the subband signal quality is examined.

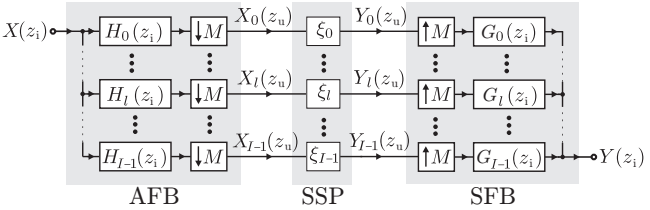

Figure 1: HI processing chain comprising FBS and SSP, $z_\mathrm{u} = z_\mathrm{i}^M$

Furthermore, we compare several approaches to the design of oversampling complex-modulated FBS, how closely they are able to meet the particular needs of FBS for HI, their pros and cons: Especially, we compare the approaches by DAM et al. [8], by STÖCKER et al. [9], by BÄUML and SÖRGEL [10] and that of the companion proposals of ALFSMANN et al. [11] and KURBIEL et al. [12]. Although the approach [8] has a powerful successor [13], we focus on [8] since the former contribution includes the FBS group delay behaviour, which is beyond the scope of this paper.

This contribution is organised as follows: In section 2, we give a brief description of oversampling complex-modulated FBS, along with findings of their behaviour regarding multirate disturbance [11]. Next, in section 3, we discuss the above approaches and assess their expected performance. Finally, we confirm our statements with a design example (section 4), followed by concluding remarks in section 5.

2. OVERSAMPLING COMPLEX-MODULATED FILTER BANK SYSTEMS

A digital processing chain utilising a general decimating FBS is depicted in Fig. 1. The FBS is composed of the analysis filter bank (AFB) and the synthesis filter bank (SFB). The input signal is sampled at frequency f_i and is represented by its spectrum $X(z_\mathrm{i})$, $z_\mathrm{i} = \mathrm{e}^{\mathrm{j}\Omega}$, $\Omega = 2\pi f/f_\mathrm{i}$ for technical frequencies f. $X(z_\mathrm{i})$ is separated into I subband spectra $X_l(z_\mathrm{u}) = X_l\left(z_\mathrm{i}^M\right)$, $l = 0,\ldots,I-1$, by filtering the input signal by I distinct analysis filters $H_l(z_\mathrm{i})$, and the AFB subband signals are downsampled by M: $f_\mathrm{u} = f_\mathrm{i}/M$. The subband signals $Y_l(z_\mathrm{u})$ at the SFB inputs are upsampled by M, filtered with I different synthesis filters $G_l(z_\mathrm{i})$ and merged to the FBS output signal $Y(z_\mathrm{i})$.

To model the SSP between AFB and SFB, an individual amplification factor ξ_l is foreseen in each subband l:

$$Y_l(z_\mathrm{u}) = \xi_l X_l(z_\mathrm{u}). \tag{1}$$

In a practical hearing aid, the SSP comprises several, in part nonlinear, processing tasks. However, we restrict ourselves to (1), because the amplification of subband signals has the greatest impact on FBS functionality, as we will justify.

2.1 Input, subband and output signals relations

In FBS based on complex (DFT) modulation, the analysis and synthesis filters are derived from the prototype filters, $H_0(z)$ and $G_0(z)$, as follows:

$$H_l(z) = H_0\left(zW_I^l\right), \quad G_l(z) = G_0\left(zW_I^l\right), \quad l = 0,\ldots,I-1, \tag{2}$$

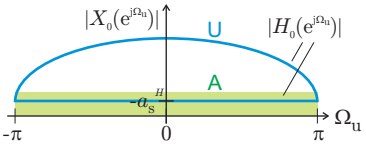

Figure 2: Usable signal (U) and aliasing (A) component within subband spectrum $X_0\left(e^{j\Omega_u}\right)$; AFB prototype attenuation a_s^H is constant

where $W_I = e^{-j\frac{2\pi}{I}}$. For minimum expenditure, the prototype filters are assumed as real-valued lowpass filters. Moreover, in practical applications, a polyphase implementation [4, 5] is used. Considering (2) and downsampling [4, 5], we get the alias component representation of the subband spectra:

$$X_l(z_u) = \frac{1}{M}\sum_{m=0}^{M-1} H_0\left(z_u^{\frac{1}{M}} W_I^l W_M^m\right) X\left(z_u^{\frac{1}{M}} W_M^m\right), \quad (3)$$

where $W_M = e^{-j\frac{2\pi}{M}}$. Applying (1), upsampling [4, 5], and (2) in conjunction with (3), the FBS output signal is given by:

$$\begin{aligned} Y(z_i) &= \sum_{l=0}^{I-1} G_0\left(z_i W_I^l\right) \xi_l X_l\left(z_i^M\right) \\ &= \frac{1}{M}\sum_{m=0}^{M-1}\left[\sum_{l=0}^{I-1} \xi_l G_0\left(z_i W_I^l\right) H_0\left(z_i W_I^l W_M^m\right)\right] X\left(z_i W_M^m\right). \quad (4) \end{aligned}$$

Splitting the outer summation in (4) into one term for $m = 0$ and those terms for $m = 1,\ldots,M-1$, and setting $z_i := e^{j\Omega}$, we define the FBS (linear) *distortion function*

$$T\left(e^{j\Omega}\right) = \frac{1}{M}\sum_{l=0}^{I-1} \xi_l G_0\left(e^{j(\Omega-\frac{2\pi}{I}l)}\right) H_0\left(e^{j(\Omega-\frac{2\pi}{I}l)}\right) \quad (5)$$

and the *aliasing function* (multirate disturbance induced by aliasing *and* imaging)

$$A\left(e^{j\Omega}\right) = \frac{1}{M}\sum_{m=1}^{M-1}\sum_{l=0}^{I-1} \xi_l G_0\left(e^{j(\Omega-\frac{2\pi}{I}l)}\right) H_0\left(e^{j(\Omega-\frac{2\pi}{I}l-\frac{2\pi}{M}m)}\right). \quad (6)$$

Both (5) and (6) are transfer functions from the FBS input to its output that are, moreover, $\frac{2\pi}{I}$-periodic [9, 12].

2.2 Basic specification

Although the investigated approaches differ in their prototype filter specification, they have the following basic properties in common. To save computational load and group delay, the design freedom of the FBS, oversampling by $\mathscr{O} = I/M$, is exploited such that the stopband edge is specified as $\Omega_s = \pm\pi/M$, the maximum value possible if aliasing and imaging have to be suppressed merely by filter attenuation. Due to this specification, always $\mathscr{O}$ subbands overlap spectrally. Furthermore, measures must be taken that $H_0(z)$ and $G_0(z)$ are approximately matched in such a way that (5) approximates an *allpass* function.

2.3 Generation of multirate disturbance

In [11], the different sources of multirate disturbance are separated. In the following, we subsume the main statements. Subsequently, the passband (including the transition band) domains of prototype filters H_0 and G_0 are denoted by $\mathbb{B}_p = [-\Omega_s, \Omega_s]$, the respective stopband frequency region by $\mathbb{B}_s = [-\pi, -\Omega_s] \cap [\Omega_s, \pi]$.

The subband signals are disturbed by aliasing, caused by downsampling in the AFB: Following (3), $M-1$ spectral contributions of the input signal are attenuated by $H_0(\mathbb{B}_s)$ and folded onto the usable subband spectrum. As an example, the signal components within a subband spectrum $X_0\left(e^{j\Omega_u}\right)$, $\Omega_u = M\cdot\Omega$, are depicted in Fig. 2: Since the usable signal component is shaped by $H_0\left(\mathbb{B}_p\right)$, the *signal-to-distortion ratio* (SDR) is not constant versus frequency Ω_u, even if a constant $H_0(\mathbb{B}_s)$ attenuation a_s^H is assumed.

The FBS signal transfer from input to output is carried out via $\mathscr{O}$ subbands, which are reshaped by $G_0\left(\mathbb{B}_p\right)$. Thus, on the one hand,

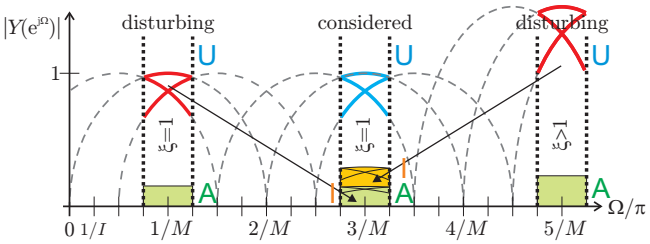

Figure 3: Usable signal (U), aliasing (A) and imaging (I) component within an output signal channel, each composed of $\mathscr{O} = 4$ overlapping, partly amplified ($\xi_l \geq 1$), subspectra of subband signals $X_l(z_u)$

we retrieve the input signal at the FBS output subjected to linear distortion (5). On the other hand, also subband aliasing is reshaped by $G_0\left(\mathbb{B}_p\right)$, which means that subspectra with lower SDR (Fig. 2) undergo higher attenuation. Hence, if we optimise the subband signal SDR_X, we will *not* optimise the output signal SDR_Y.

The output signal also exhibits imaging components caused by upsampling. For each reconstructed usable signal component (which is shaped by $H_0\left(\mathbb{B}_p\right)$ and transferred via $\mathscr{O}$ subbands), $M-1$ images are attenuated with $G_0\left(\mathbb{B}_s\right)$ and copied onto different frequency locations: Fig. 3. Moreover, and in contrast to common FBS assumptions, we incorporate the subband signal amplification in the SSP: ξ_l in (6). At the same time, this amplification can be very high (up to 60dB), and the differences between amplification factors can be enormous [3, 10]. Hence, severe disturbance in the less amplified output signal subspectra are caused (Fig. 3). As a consequence, subband signal amplification has an utmost impact on the multirate disturbance (*here:* imaging) generated within the FBS.

Summary [11]: The *significant* signal degradation in the FBS from input port to output port is effected by

1. *aliasing*, shaped by $H_0\left(\mathbb{B}_s\right)$ and $G_0\left(\mathbb{B}_p\right)$ and
2. *imaging*, shaped by $G_0\left(\mathbb{B}_s\right)$, ξ_l and $H_0\left(\mathbb{B}_p\right)$.

3. DISCUSSION OF APPROACHES

We firstly evaluate each approach [8, 9, 10, 11, 12] separately, applying a harmonised notation. Note that all approaches meet the basic requirements of Sec. 2.2.

3.1 Approach by DAM et al. [8]

In the first part of [8], no assumptions are made regarding the input signal and SSP ("minimum knowledge"), besides that the latter is expected to consist of arbitrary linear transfer functions.

Two different optimisation objectives are defined: Minimisation of disturbance within the subband signals ("inband aliasing") and within the output signal ("residual aliasing"). To reduce aliasing within the subbands, H_0 can be optimised by minimising

$$A_{\mathrm{inband}} = \frac{1}{2\pi M^2}\sum_{m=1}^{M-1}\int_{-\pi}^{\pi}\left|H_0\left(e^{j\frac{\Omega}{M}} W_M^m\right)\right|^2 d\Omega, \quad (7)$$

which represents the overall aliasing power in subband $l = 0$; cf. (3). This is feasible because the input to subband relations (3) of every subband are equivalent. It should be pointed out that in (7) all aliasing portions are superimposed with the squares of their magnitudes. This implies that these portions are assumed uncorrelated, a reasonable approximation [11].

A similar derivation is made from (6) to get a measure of the output signal disturbance

$$A_{\mathrm{res}} = \frac{1}{2\pi M^2}\sum_{m=1}^{M-1}\sum_{l=1}^{I-1}\int_{-\pi}^{\pi}\left|H_0\left(e^{j\frac{\Omega}{M}} W_I^l W_M^m\right) G_0\left(e^{j\frac{\Omega}{M}} W_I^l\right)\right|^2 d\Omega, \quad (8)$$

which is used to optimise H_0 and G_0. Here, the SSP is characterised by $\xi_l \equiv 1$, $l = 0,\ldots,I-1$.

Both (7) and (8) are reformulated to serve as objective functions of a constrained quadratic optimisation problem in dependence of the filter coefficients. For optimisation of H_0, a linear combination of (7) and (8) is used applying an adjustable weight v. For optimisation of G_0, only the reformulation of (8) is used as the objective function. An iterative algorithm allows for virtually simultaneous optimisation of both H_0 and G_0. The optimisation is constrained by the observation of the distortion function (5) versus frequency:

$$\left|T\left(\mathrm{e}^{\mathrm{j}\Omega}\right) - T_d\left(\mathrm{e}^{\mathrm{j}\Omega}\right)\right| \leq \varepsilon(\Omega), \quad T_d\left(\mathrm{e}^{\mathrm{j}\Omega}\right) = \mathrm{e}^{-\mathrm{j}\Omega\tau_d}, \qquad (9)$$

where $\varepsilon(\Omega)$ is the frequency-dependent error and τ_d the desired group delay. Constraints are generally set in the range $\Omega \in [-\pi, \pi]$, but it is proved that if $\tau_d = \iota I$, $\iota \in \mathbb{N}$, this range can be reduced to $\Omega \in [-0, 2\pi/I]$. No stringent condition is set on the filter lengths, but $N = \iota I$ is recommended, suggesting equal filter lengths for H_0 and G_0: $N^H = N^G$.

3.2 Approach by STÖCKER et al. [9]

The approach [9] is a modification of [8]. First of all, the supplementary assumptions are more restricted. In [9], the input signal is assumed to be white and the SSP to be transparent. However, this does not disagree with the objective functions used in [8] for the final filter design. Furthermore, in [9], only the disturbance within the output signal is minimised. In comparison with (8), the error function is simplified such that summation over all l subbands is omitted:

$$A_{\mathrm{res}} = \frac{1}{\pi M} \sum_{m=1}^{M-1} \int_{\Omega_1}^{\Omega_2} \left|H_0\left(\mathrm{e}^{\mathrm{j}\left(\Omega - \frac{2\pi}{M}m\right)}\right) G_0\left(\mathrm{e}^{\mathrm{j}\Omega}\right)\right|^2 d\Omega, \qquad (10)$$

which is possible without disregarding any disturbance component as a result of the $2\pi/I$-periodicity. Moreover, the limits of the integral over Ω are adapted to the respective dominating function of H_0 and G_0, following Sec. 2.3: For optimisation of H_0, the limits are set to $\Omega_1 = 0, \Omega_2 = \Omega_{\mathrm{s}} = \pi/M$, which means that (10) measures solely aliasing: $H_0(\mathbb{B}_{\mathrm{s}})$ and $G_0\left(\mathbb{B}_{\mathrm{p}}\right)$. For minimisation of imaging by optimising G_0, the limits of (10) are set to $\Omega_1 = \Omega_{\mathrm{s}}, \Omega_2 = \pi$, which considers only the stopband of G_0. However, the complete transfer function H_0 has an effect on (10).

For the actual filter optimisation, both alternatives of (10) are reformulated such that they can be optimised alternately by a constrained quadratic procedure. The constraints are again given by (9) and provide a reasonable distortion function (5). Since the design problem is proved to be convex, the starting coefficients can be random. However, the filter lengths N^H, N^G have to be chosen in advance. Here, no statement is given beyond [8].

3.3 Approach by BÄUML and SÖRGEL [10]

Similarly to [8, 9], in [10] an SSP is mentioned (and stated more precisely with subband signal amplification profiles), but not used for the actual filter design. To determine the output signal disturbance, a frequency-dependent distortion-to-signal ratio criterion

$$R\left(\mathrm{e}^{\mathrm{j}\Omega}\right) = \frac{\sum_{m=1}^{M-1}\sum_{l=0}^{I-1}\left|H_0\left(\mathrm{e}^{\mathrm{j}\left(\Omega+\frac{2\pi}{I}l+\frac{2\pi}{M}m\right)}\right) G_0\left(\mathrm{e}^{\mathrm{j}\left(\Omega+\frac{2\pi}{I}l\right)}\right)\right|^2}{\sum_{m=0}^{M-1}\sum_{l=0}^{I-1}\left|H_0\left(\mathrm{e}^{\mathrm{j}\left(\Omega+\frac{2\pi}{I}l+\frac{2\pi}{M}m\right)}\right) G_0\left(\mathrm{e}^{\mathrm{j}\left(\Omega+\frac{2\pi}{I}l\right)}\right)\right|^2} \qquad (11)$$

is defined, which can be derived from (4-6): The numerator contains all aliasing and imaging components, the denominator the overall (usable and disturbance) signal, SSP is transparent: $\xi_l \equiv 1$. The signal portions are superimposed by their squared magnitudes , which means that they are assumed uncorrelated.

To set up an objective function, a linear combination of the mean and the maximum value of (11)

$$A_{\mathrm{res}} = \frac{1}{\pi}\int_0^{\pi} R\left(\mathrm{e}^{\mathrm{j}\Omega}\right) d\Omega + \lambda \max_{\Omega} R\left(\mathrm{e}^{\mathrm{j}\Omega}\right), \qquad (12)$$

is composed by using a weight parameter λ. Using a classic perfect reconstruction filter bank prototype design approach as initial solution, only one prototype filter is optimised with regard to the objective (12), while the other one is derived by time-domain flipping of the former impulse response (minimum- / maximum-phase filter pair). The optimisation is carried out by a simulated annealing (SA) procedure. The filter lengths are arbitrary, but due to the described relation between AFB and SFB prototype filter, $N^H \equiv N^G$ is prescribed.

3.4 Approach by ALFSMANN [11] and KURBIEL [12]

This approach consists of two parts: Requirements and FBS specification [11], and actual filter design [12] approximating them.

In [11], a white FBS input spectrum is assumed, and distinct amplification factors ξ_l are applied to each subband l. The $\xi_l \geq 1$ can be adapted to an individual hearing loss or an assumed worst-case amplification profile. The objective of this approach is to guarantee a prescribed output SDR independently of any given subband signal amplification within prescribed limits.

A major difference compared to the approaches [8, 9] is that the roles of objective function and optimisation constraints are interchanged. Starting with the design [12] of either H_0 or G_0, an objective function for group delay is stated. Then, to build a suitable filter bank pair, the objective function needed for optimisation of the respective other filter prototype is determined as a reformulation of (9). Each design represents a constrained quadratic problem.

For optimisation of H_0 and G_0, separate constraints for the magnitude transfer functions $|H_0|$ and $|G_0|$ are developed to maintain the prescribed output signal SDR. According to Sec. 2.3, both filters H_0 and G_0 have impact on the multirate disturbance. However, in [11] only the stopbands $H_0(\mathbb{B}_{\mathrm{s}})$ and $G_0(\mathbb{B}_{\mathrm{s}})$ are constrained to control the disturbance, to leave freedom within $H_0\left(\mathbb{B}_{\mathrm{p}}\right)$ and $G_0\left(\mathbb{B}_{\mathrm{p}}\right)$ for the objective functions (distortion function or group delay) [12]. To keep the number of constraints tractable, they are defined on frequency intervals $\Omega_c = \left[(2c-1)\frac{\pi}{I}, (2c+1)\frac{\pi}{I}\right]$, where $c \in \left\{\left\lceil\frac{\mathscr{O}}{2}\right\rceil, \ldots, \left\lfloor\frac{I}{2}\right\rfloor\right\}$ is the index of the frequency-dependent constraints within the respective stopband. For optimisation of H_0, each constraint

$$a_{\mathrm{s}}^H(c) = a_{\mathrm{s}}^H + a_{\mathrm{s,o}}^H(c) + a_{\mathrm{s,m}}^H(c), \qquad (13)$$

noted in dB, is the logarithmic summation of the bias (uniform) attenuation a_{s}^H, and two refining frequency-dependent attenuations $a_{\mathrm{s,o}}^H(c)$ and $a_{\mathrm{s,m}}^H(c)$, controlling major aliasing contribution. For SFB prototype design and to control imaging, each constraint

$$a_{\mathrm{s}}^G(c) = a_{\mathrm{s}}^G + a_{\mathrm{s,o}}^G(c) + a_{\mathrm{s,m}}^G(c) + a_{\mathrm{s,g}}^G(c) \qquad (14)$$

is refined with three frequency-dependent attenuations. The bias attenuations

$$a_{\mathrm{s}}^{\bullet} = \mathrm{SDR} - 10\log_{10}\left(\frac{\sum_{\kappa=-K+1}^{K-1}\gamma_\kappa^2\beta_\kappa^2 + q\gamma_K^2\beta_K^2}{[M-1]\sum_{\kappa=-K}^{K}\delta_\kappa^2}\right) + 3\mathrm{dB}, \qquad (15)$$

$$\beta_\kappa^2 = \frac{I}{2\pi}\int_{\Omega_1}^{\Omega_2}\left|H_0\left(\mathrm{e}^{\mathrm{j}\Omega}\right)\right|^2 d\Omega, \quad \gamma_\kappa^2 = \frac{I}{2\pi}\int_{\Omega_1}^{\Omega_2}\left|G_0\left(\mathrm{e}^{\mathrm{j}\Omega}\right)\right|^2 d\Omega, \qquad (16)$$

$q = 2$ ($q = 4$) if $\mathscr{O}$ is odd (even), $\Omega_1 = (2\kappa-1)\frac{\pi}{I}$, $\Omega_2 = (2\kappa+1)\frac{\pi}{I}$, $\kappa \in \{-K, \ldots, K\}$, $K = \left\lfloor\frac{\mathscr{O}}{2}\right\rfloor$, are determined by estimation of the output usable signal power in relation to the aliasing power by applying $\delta_\kappa = \gamma_\kappa$ in (15) yielding a_{s}^H, or to the imaging power by applying $\delta_\kappa = \beta_\kappa$ in (15) yielding a_{s}^G, respectively. With (15), uncorrelated superposition of signal, aliasing and imaging contributions is assumed to approximate their undefined correlation.

An example specification (*here:* for $G_0(\mathbb{B}_{\mathrm{s}})$) is depicted in Fig. 4. The frequency-dependent attenuations $a_{\mathrm{s,o}}^{\bullet}(c)$ in (13), (14) are specified $\mathscr{O}$-periodic regarding the parameter c ($\frac{2\pi}{M}$-periodic "lobes" in Ω, cf. Figs. 5,6). They are used to compensate differing power of aliasing or imaging contributions at the respective frequency locations Ω_c, resulting from $\mathscr{O} > 1$. To incorporate an audiological frequency masking effect, the attenuations $a_{\mathrm{s,m}}^{\bullet}(c)$ in (13), (14) allow for considering a *lower* attenuation at frequencies

near to the transition region of the respective prototype filter. In contrast, the frequency-dependent attenuation $a^G_{\mathrm{s,g}}(c)$ in (14) *increases* the stopband attenuation in distinct channels c, and is adapted to the prescribed amplification profile ξ_l.

The filter lengths N^H and N^G must be determined independently by the actual filter design [12]. When considering subband signal amplification, in general there is $N^G > N^H$.

3.5 Assessment of approaches

Subsequently, we compare the described approaches as to their potential of aliasing and imaging suppression within the FBS output signal. In Sec. 2.3, the respective dependencies on FBS prototype filter characteristics and ξ_l have been outlined. Note that the objective functions of [8, 10] always commonly deal with aliasing and imaging. In contrast, the constraints in [11] are derived from the observations of Sec. 2.3. Likewise, this applies to the objective functions (10) of [9] apart from the dependence of $G_0(\mathbb{B}_\mathrm{s})$ optimisation on $H_0(\mathbb{B}_\mathrm{s})$. Separation of aliasing and imaging contributions has the potential of effective filter design [9]. The principal difference of [11] to the other approaches is the consideration of amplification factors $\xi_l \geq 1$ for $G_0(\mathbb{B}_\mathrm{s})$ design, to compensate for the impact of amplified imaging contributions on the output signal quality. The significance of this effect has been substantiated in Sec. 2.3 and will be confirmed in Sec. 4.

None of the approaches uses exact calculation of multirate disturbance: An uncorrelated superposition of aliasing and imaging contributions is expected. Moreover, in [11], the magnitude responses are approximated by coarse piecewise constant values. However, this approach allows for prescribing a distinct output SDR, which is not possible with all other approaches.

The approaches [8, 9, 11] state a constrained *convex* quadratic optimisation problem, i.e. the global optimum is always found regardless of the starting coefficients. In contrast, design results obtained by applying simulated annealing, as used in [10], are, with finite calculation time, highly dependent on the initial coefficients. However, this method can be used for discrete coefficient optimisation [10].

4. EXAMPLE

As an example, we consider a HI FBS with $I = 64$ uniform subbands in $\Omega \in [0, 2\pi]$ and decimating with $M = 16$ ($\mathscr{O} = 4$). It is designed with the approaches [8, 9, 11, 12]. The input signal is assumed to have a white spectrum $X \equiv 1$, the subband signal amplification to have a "ski-slope" [10] profile $\xi_l = 1$, $l \leq 10$, $\xi_l = 10^{\frac{l-10}{8}\cdot\frac{60}{20}}$, $10 \leq l \leq 18$, and $\xi_l = 10^{\frac{60}{20}} = 1000$, $18 \leq l \leq 32$, with even symmetry about $\Omega = \pi$: $\xi_l = \xi_{64-l}$, $l = 33, \ldots, 63$. We aim at an FBS output $\mathrm{SDR}_Y = 50$dB independent of subband signal amplification within the range of the prescribed profile.

Starting with [11], an SDR_Y postulation rather than filter length specification is required. In Fig. 4, the composition of the frequency-dependent specification (14) for $G_0(\mathbb{B}_\mathrm{s})$ is depicted. While the bias attenuation (15) and the oversampling component $a^G_{\mathrm{s,o}}(c)$ are determined by prescribed SDR_Y and the initial $H_0(\mathbb{B}_\mathrm{p})$, the amplification component $a^G_{\mathrm{s,g}}(c)$ is adapted to the slope of ξ_l. To get comparable results, we do not exploit a masking effect and set: $a^G_{\mathrm{s,m}} \equiv 0$dB. $H_0(\mathbb{B}_\mathrm{s})$ is specified accordingly.

The magnitude responses of the prototype filters H_0 and G_0, designed according to [12], are depicted in Figs. 5 and 6 along with the respective constraining stopband specification $a^\bullet_\mathrm{s}(c)$: Ex. A. The resulting filter lengths are $N^H = 75$ and $N^G = 109$. Next, we design filters according to [8] (Ex. B) and [9] (Ex. C) with identical filter lengths of the AFB and SFB prototypes. Prescribing $N^H = N^G = 92$, we maintain the same overall FBS expenditure as that of Ex. A. Furthermore, we aim for a magnitude of the distortion function within ± 0.1dB. Finally, for [8] (Ex. B), we set the weight to $v = 0$ in order to optimise for maximum FBS output SDR.

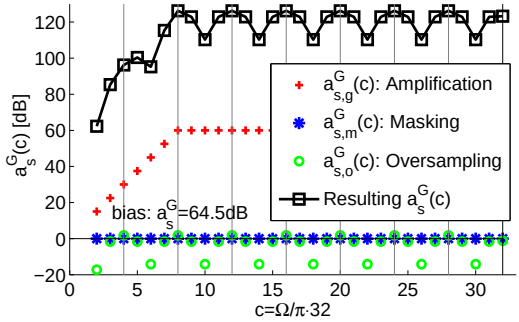

Figure 4: Composition of specification $a^G_\mathrm{s}(c)$ (Ex. A)

Ex.	App.	N^H	N^G	SDR_X [dB]	Dist. [dB]	SDR_Y [dB]	
						$\xi_l \equiv 1$	$\xi_l \geq 1$
A	[11]	75	109	46.0	±0.3	49.7	49.6
B	[8]	92	92	61.5	±0.2	80.4	31.8
C	[9]	92	92	55.3	±0.2	76.7	30.3
D	[8]	75	109	38.3	±0.02	77.0	32.3
E	[9]	75	109	39.1	±0.2	73.2	38.4
F	[9]	55	129	27.5	±0.2	53.8	49.9

Table 1: Simulation results of Ex. A-F (always $N^H + N^G = 184$)

Although only for Ex. A, $\frac{2\pi}{M} = \frac{\pi}{8}$-periodic lobes are specified for $H_0(\mathbb{B}_\mathrm{s})$ and $G_0(\mathbb{B}_\mathrm{s})$, we observe from Figs. 5 and 6 that also Ex. B and Ex. C possess this property (all designs exhibit $\frac{M}{2} - 1 = 7$ lobes within $\mathbb{B}_\mathrm{s}$). Even by [10], these lobes are obtained. Obviously, these lobes follow from FBS output SDR_Y optimisation, based on the respective objective function (8), (10) and (11).

We evaluate the designs Ex. A-C with the noise power ratio simulation method [14]. Thus, the FBS output SDR_Y is determined both with and without the prescribed amplification profile: Fig. 7 (*here:* Ex. B). Also, the subband signal disturbance is simulated: Fig. 8. In contrast to Fig. 2, the lobes in $H_0(\mathbb{B}_\mathrm{s})$ (*here:* Ex. C) shape the aliasing within the subband.

The simulation results are summarised in Tab. 1: Obviously, with the design Ex. A the specification $\mathrm{SDR}_Y = 50$dB is well approximated within the range of the prescribed amplification profile ξ_l: $\mathrm{SDR}_Y \approx 49.7$dB. By comparison, Ex. B(C) exhibits a much better $\mathrm{SNR}_Y = 80.4(76.7)$dB in the case of *transparent* SSP, while only $\mathrm{SNR}_Y \approx 66$dB is obtained by [10]. However, by applying the prescribed subband signal amplification, the output signal quality falls off significantly: $\mathrm{SDR}_Y = 31.8(30.3)$dB. This difference is due to the fact that, in [8, 9], no SSP is assumed and, hence, the same expenditure is spent for AFB and SFB. In contrast, with the same overall FBS expenditure, the SFB of Ex. A [11] is more complex than the AFB and, particularly, than both filter banks of Ex. B,C: Cf. Figs. 5 and 6. On the other hand, the AFB of Ex. A is rather simple and, in case of $\xi_l \equiv 1$, yields a worse SNR_Y compared to Ex. B,C.

To check if the distribution of AFB and SFB complexity of Ex. A is also beneficial for the approaches [8, 9], we redesign Ex. B,C using $N^H = 75$, $N^G = 109$: Ex. D,E (Tab. 1). With the amplification profile, Ex. E [9] has obtained a much better $\mathrm{SDR}_Y = 38.4$dB, whereas Ex. D [8] is only slightly improved to $\mathrm{SDR}_Y = 30.3$dB. With both redesigns, the performance of Ex. A with $\mathrm{SDR}_Y = 49.6$dB is not achieved. By fixing the overall expenditure to $N^H + N^G = 184$, it was possible to achieve $\mathrm{SDR}_Y = 49.9$dB by using [9]: Ex. F, $N^H = 55$, $N^G = 129$. As a result, only a low subband $\mathrm{SDR}_X = 27.5$dB is obtained, which is due to the low AFB filter order. Similar results could not be accomplished with approach [8]. With Ex. A, in case of $\xi_l \geq 1$, $\mathrm{SDR}_Y = 49.6$dB can be achieved with a simpler SFB than for Ex. F, because the slope of the amplification profile is accurately considered in the specification (Fig. 4). As a consequence, as to be seen from Fig. 6, the maximum attenuation $a^G_\mathrm{s} \approx 120$dB is reached not before $\Omega = 0.2\pi$, widening the critical transition band.

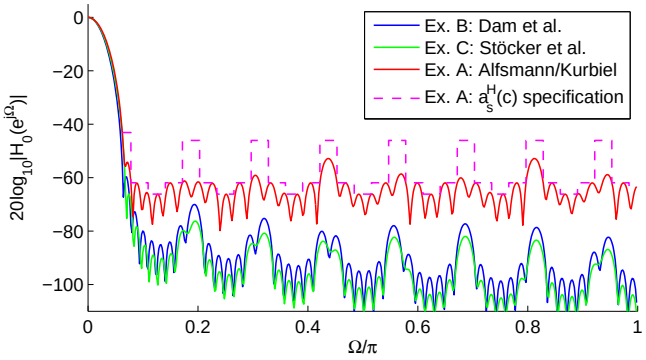

Figure 5: Magnitude responses $\left|H_0\left(e^{j\Omega}\right)\right|$ (Ex. A-C)

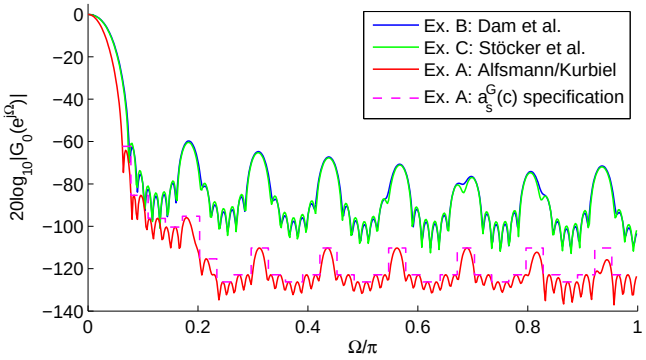

Figure 6: Magnitude responses $\left|G_0\left(e^{j\Omega}\right)\right|$ (Ex. A-C)

5. CONCLUSION

We have investigated the dependencies of aliasing and imaging generation within FBS, and have analysed the impact of subband signal amplification on FBS output signal quality for HI applications. To keep multirate disturbance by imaging within tolerable limits, it is *indispensable* to design the SFB for a stopband attenuation exceeding that of the AFB. As a result, SFB expenditure must generally be higher than that of the AFB. Although we have not considered the reduced usable dynamic range of a hearing impaired person within our framework, we point out that the impact of imaging is most severe on the (healthy) less amplified subspectra.

It has been demonstrated that the approach [11] is capable of providing a *prescribed* FBS output SDR *independent* of subband signal amplification within a given range of amplification. This is achieved by applying coarse, piecewise constant stopband magnitude constraints to the AFB and SFB prototype filter design. However, as to be seen from Figs. 5 and 6 (Ex. A [11]), especially the shorter (AFB) filters cannot fully exploit the stopband design margin and, hence, tend to some excess filter order as compared to the designs according to [8, 9]. A further advantage of the approach [8] is that it also allows for optimising the subband signals' quality.

When it comes to the case $\xi_l \geq 1$, only [11, 12] can provide appropriate FBS prototype filter designs. Moreover, the approach has the potential to consider additional impact on signal quality (e.g. masking effects). Beyond that proposal, especially the approach [9] has the potential to be adapted to extensive SSP: cf. Tab. 1, Ex. F.

For all approaches, future research has to investigate the impact of real-world input signal dynamics on the FBS functionality.

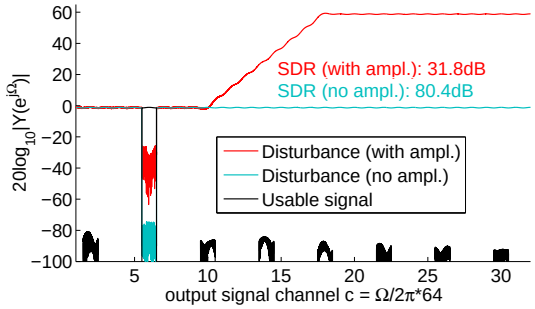

Figure 7: Simulation of output SDR_Y (Ex. B)

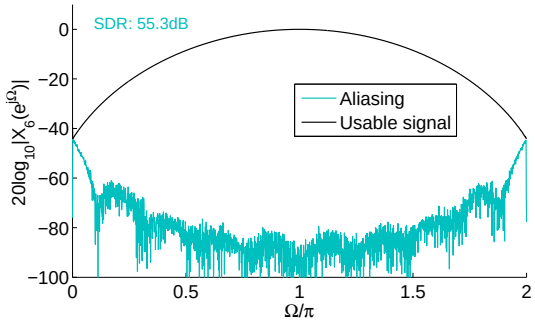

Figure 8: Simulation of subband signal SDR_X (Ex. C)

REFERENCES

[1] V. Hamacher, J. Chalupper, J. Eggers, E. Fischer, U. Kornagel, H. Puder, and U. Rass, "Signal processing in high-end hearing aids: State of the art, challenges, and future trends," *J. Applied Signal Process.*, vol. 18, pp. 2915–2929, 2005.

[2] E. Hänsler and G. Schmidt, Eds., *Speech and Audio Processing in Adverse Environments*, Springer-Verlag, Berlin, 2008.

[3] H. Dillon, *Hearing Aids*, Thieme, New York, 2001.

[4] P. P. Vaidyanathan, *Multirate Systems and Filter Banks*, Prentice Hall, Englewood Cliffs, New Jersey, 1993.

[5] H. G. Göckler and A. Groth, *Multiratensysteme*, Schlembach Fachverlag, Willburgstetten, Germany, 2004.

[6] J. Chalupper and H. Fastl, "Dynamic loudness model (DLM) for normal and hearing-impaired listeners," *Acta Acustica united with Acustica*, vol. 88, no. 3, pp. 378–386, 2002.

[7] A. Leijon, "Hearing aid gain for loudness-density normalization in cochlear hearing losses with impaired frequency resolution," *Ear & Hearing*, vol. 12, no. 4, pp. 242–250, 1990.

[8] H. H. Dam, S. Nordholm, A. Cantoni, and J. M. de Haan, "Iterative method for the design of DFT filter bank," *IEEE Trans. on Circuits and Systems–II: Express Briefs*, vol. 51, no. 11, pp. 581–586, November 2004.

[9] C. Stöcker, T. Kurbiel, D. Alfsmann, and H. G. Göckler, "A novel approach to the design of oversampling complex-modulated digital filter banks," *this proceedings*, 2009.

[10] R. W. Bäuml and W. Sörgel, "Uniform polyphase filter banks for use in hearing aids: Design and constraints," in *European Signal Processing Conf. (EUSIPCO'08)*, Lausanne, Switzerland, 2008.

[11] D. Alfsmann, H. G. Göckler, and T. Kurbiel, "Frequency domain constraints to oversampling filter bank systems in hearing aids to ensure a prescribed output signal-to-distortion ratio," *accep. for pub. in JASP Advances in Signal Processing*.

[12] T. Kurbiel, H. G. Göckler, and D. Alfsmann, "A novel approach to the design of oversampling low-delay complex-modulated filter bank pairs," *accepted for publication in Journal on Advances in Signal Processing (JASP)*.

[13] H. H. Dam, S. Nordholm, and A. Cantoni, "Uniform FIR filterbank optimization with group delay specifications," *IEEE Trans. on Sig. Proc.*, vol. 53, no. 11, pp. 4249–4260, 2005.

[14] H. G. Göckler and T. Gebauer, "Model-based simulation of a class of digital FDM-demultiplexers in beamforming environment," *Proc. Intern. Conf. Dig. Satellite Comm., Copenhagen, Denmark*, vol. ICDSC-9, pp. Band A, S.311–318, 1992.